Computational Analysis of Convective Heat Transfer Across a Vertical Tube

Jashanpreet Singh
Assistant Professor
Department of Engineering
Punjab State Aeronautical Engineering College, Patiala, Punjab
India

Chanpreet Singh
Professor
Department of Mechanical Engineering
Punjabi University, Patiala, Punjab
India

This paper deals with the numerical investigation of the convective mode of heat transfer across a vertical tube. Experiments were carried out using air as a fluid in a closed room by achieving a steady-state condition. Implicit scheme of finite difference method was adopted to numerically simulate the free convection phenomenon across vertical tube using LINUX based UBUNTU package. Numerical data were collected in the form of velocity, temperature profiles, boundary layer thickness, Nusselt number (Nu), Rayleigh's number (Ra), and heat transfer coefficient. The results of the Nusselt number showed a good agreement with the previous studies. Results data of heat transfer coefficient indicate that there were some minor heat losses due to radiation of brass tube and curvature of the tube.

Keywords: *Natural convection, vertical tube, Boundary layer, Finite difference method, heat transfer, Nusselt number, Grashof number.*

1. INTRODUCTION

Convection is a branch of heat transfer that deals with a variety of engineering applications like heat exchangers, green–house effect generators, radiators, condensers, air conditioners, refrigerators, electronics, etc. [1,2]. Numerous numerical and experimental studies were carried out by various researchers to investigate the free convection phenomenon across the horizontal and vertical cylinders [3–7]. However, methane gas is used in applications such as energy storage devices and reactors [8]. Methane is generally stored in liquid a form. The applications of methane in different industries are in the manufacturing of organic chemicals, used as refrigerated liquid, to run the power engines and turbines, in automobiles, ovens and water heaters, greenhouse effect generators, etc. However, during the transferring or conveying process, the metallic cylinders get heated on the surfaces. In this context, the boundary layer phenomenon plays a crucial role.

In the previous study, Blottner [9] numerically studied the boundary layer equations by a finite dif–fe–rential method (FDM). Acharya et al. [3] performed a numerical study to investigate the free convection phe–nomenon for the heat transfer from a vertical hollow cylinder. They used the fluid air to conduct the nu–merical simulation. They found that the Nusselt number (*Nu*) was increased with the increase in the Rayleigh number (*Ra*). Moreover, *Nu* was increased linearly with the increase in length-to-outer diameter (L/D_o) and decrease in the length-to-outer diameter (L/D_i). Arshad et al. [4] studied the heat transfer for the stationary water passing through a vertical cylinder. They found that the surface temperature of the water with respect to time was increased while passing through a narrow annular space hat sink and an increase in temperature was observed more as compared to the water passing through a wide annular space heat sink. In order to evaluate natural convection laminar flow, Saha and Hossain [10] conducted a numerical investigation on a vertical cylinder. The governing equation was deter–mined by an implicit scheme of the FDM and local non-similarity schemes. They found that the buoyant forces were developed by the mass and thermal diffusion in the stable thermally stratified medium across the vertical cylinder. Results demonstrated different facets of a dy–namic complex activity of the buoyancy mechanisms. Fahiminia et al. [11] investigated the laminar free convection by an FVM implicit scheme using CFD simulations. The flow domain was resolved in the presence of gradients of density on vertical surfaces under the effect of gravity. Results revealed that fin array heat transfer rates depend on fine height, weight, and spacing as well as the temperature difference between base and ambient conditions. Corasaniti and Gori [12] performed an investigation on the free con–vection around a vertical tube dipped in a porous media. Results showed that the value of the *Nu* increases as the value of *Ra* increases. Crane [13] studied the free convection across a vertical cylinder subjected to very large Prandtl numbers. They mentioned that the curva–ture effects were observed as zero for the different values of vertical locations on the cylinder (x). Dash and Dash [14] performed a numerical investigation on free convection heat transfer across a hollow vertical cylindrical tube subjected to air. They found that the average value of *Nu* was increased with L/D_o however attain a maximum value then decreased to a minimum then further increased with L/D_o. Results also depicted that the *Nu* at the inner surface was found lower than that of outer surface. Deka et al. [15] studied the transient free convection across a cylindrical tube positioned in vertical direction at a constant heat flux and conserved mass. They found that with the time increases, there is an unbound increase in the values of velocity and temperature however the fluid's concent–

Received: May 2021, Accepted: September 2021
Correspondence to: Dr Jashanpreet Singh, Department of Engineering, Punjab State Aeronautical Engineering College, Patiala, Punjab, India
E-mail: jashanpreet.singh@mrsptu.ac.in
doi:10.5937/fme2104932S

ration reaches to a steady state condition after the passage of long time periods. Senapati et al. [16] nume–rically studied the natural convection from a cylinder with annular fins positioned in vertical direction using a FLUENT ANSYS code. They found that the *Nu* was increased with the increase in fin spacing-to-tube's diameter (*S/D*) ratio and *Ra*.

From the literature, it can be said that few studies deal with the simulation of convective heat transfer using programming languages. Moreover, the flow of methane gas inside and outside can cause serious damages at room temperature. On the other hand, the practical experimentation using methane gas is practically very complex and nearly impossible in actual environmental conditions. So, there is a need to perform a numerical simulation study to investigate the natural convection phenomenon for methane. In this work, the LINUX-based UBUNTU package was used to code the free convection along a vertically hanged tube using a FORTRAN language. In this study, methane was taken as the fluid for numerical simulations. However, the experiments were performed for air by achieving a steady-state condition. The FORTRAN code was validated for the experiments of air then utilized for the methane. Parameters like velocity, temperature profiles, boundary layer thickness, Nusselt number (*Nu*), Rayleigh's number (*Ra*), and heat transfer coefficient were investigated in the present study.

2. NUMERICAL MODELING

2.1 Mathematical model

Mathematical modeling was done in order to discretize the governing equations of conservation of continuity, energy, and momentum. The discretized equations are used to generate the computer code in FORTRAN 95 language while subjected to adequate boundary condi–/tions. From this computer code, numerical data comes out on the terminal as an output. Fig. 1 shows a two-dimension coordinate system model (x, y) in the area across a cylindrical tube positioned in the vertical direction. Letters 'Q' and 'u' symbolize the flow of heat and velocity respectively. Numerical model was pre–pared for the cylindrical tube of length (l) = 0.504 m and diameter (d) = 0.038 m. The governing equations are written as:

$$\frac{\partial v}{\partial y}+\frac{\partial u}{\partial x}=0 \tag{1}$$

$$u\frac{\partial u}{\partial x}=g\beta\left(T-T_a\right)-v\left(\frac{\partial^2 u}{\partial y^2}\right)-v\frac{\partial u}{\partial y} \tag{2}$$

$$u\frac{\partial T}{\partial x}=\alpha\left(\frac{\partial^2 u}{\partial y^2}\right)-v\frac{\partial T}{\partial y} \tag{3}$$

where, Eq. (1), (2), and (3) are the governing continuity, momentum, and energy equations respectively. An implicit finite difference scheme was adopted to solve the governing equations. In this scheme, the Taylor series expansion was followed to solve the equations [17]. The approach used for solving the equations was combined in a manner i.e. combination of both Forward difference and Central difference algorithms. Central differentiation was used for the partial derivatives of y and forward differentiation was used for derivatives of x. The discretized equations are written as:

- Discretised continuity equation:

$$v_{i+1,j+1}=v_{i+1,j-1}-2\frac{\Delta y}{\Delta x}\left[u_{i+1,j}-u_{i,j+1}\right] \tag{4}$$

- Discretised momentum equation:

$$u_{i+1,j}=\frac{u_{i,j}-\dfrac{v_{i,j}}{u_{i,j}}.\dfrac{\Delta x}{\Delta y}\left[u_{i+1,j+1}-u_{i+1,j-1}\right]+\dfrac{\beta g\Delta x\left[T_{i,j}-T_a\right]}{u_{i,j}}+\dfrac{v\Delta x}{u_{i,j}.\Delta y^2}\left[u_{i+1,j+1}-u_{i+1,j-1}\right]}{\left[1+2v\Delta x\big/\Delta y^2 u_{i,j}\right]} \tag{5}$$

- Discretised energy equation:

$$T_{i+1,j}=\frac{\dfrac{\alpha\Delta x}{u_{i,j}.\Delta y^2}\left[T_{i+1,j+1}+T_{i+1,j-1}\right]-\dfrac{v_{i,j}}{u_{i,j}}.\dfrac{\Delta x}{2\Delta y}\left[T_{i+1,j+1}-T_{i+1,j-1}\right]}{\left[1+2\alpha\Delta x\big/2\Delta y^2 u_{i,j}\right]} \tag{6}$$

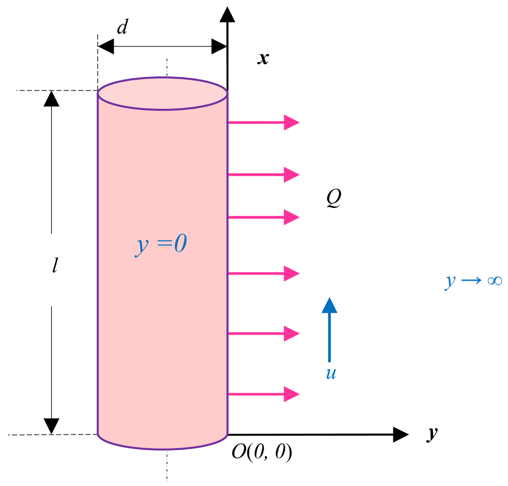

Figure 1. Two-dimensional coordinate system model (*x*, *y*) in the area across a cylindrical tube positioned in the vertical direction

Truncated or discretized Eq. (4) to (6) were used to generate a FORTRAN 95 code. Truncated forms of go–verning equations were imposed following boundary conditions:

$$y=0, T=T_s, u=0, v=0 \tag{7}$$

In this equation, the $y = 0$ indicates the no-slip boundary condition that indicates the region of initiation of the boundary layer.

$$y \to \infty, T = T_a, u \to 0, v \neq 0 \tag{8}$$

In Eq. (8), value y approaches to ∞ represent the free slip condition for the faraway region.

2.2 Computational domain

The computation domain was developed in the FORTRAN 95 programming language. The typical grid used in the present study is Fig. 2. Before simulations, a grid independency test was conducted for $m \times n$ sized grids of 1001×51, 1001×101, and 2001×101 cells. The balanced grid of size $m \times n$ was chosen for 1001×101 cells. The size of the grid was round-off to 0.5 (leng–thwise) and 0.04 (widthwise) to avoid the complexity and to produce results according to the actual para–meters. The points in 2D space across the tube in the x and y-axis are represented by the symbol 'i' and 'j' respectively. The range of 'i' was taken as 1 to n+1 whereas 1 to m+1 for 'j'. Computation model was pre–pared for the cylindrical tube of length (l) = 0.504 m and diameter (d) = 0.038 m. For the numerical simulations, a LINUX Ubuntu 2.6.321 machine was used. For the numerical simulations, a LINUX-based Ubuntu 2.6.321 operating system was used. The Gauss-Seidel iterations were used to solve the governing equations. The CPU time required to single run was noted as 10 to 15 sec.

3. EXPERIMENTS

Experiments were conducted by using the equipment shown in Fig. 3. The experiments were conducted in a closed room that was free from the influence of air. During the experiments, the temperature of the tube's surface was measured at a steady-state condition on eight different locations where the RTD PT-100 type sensors were fixed. The experimental readings were taken after achieving the steady-state condition which took approximately 3 hours. The average temperature of tube surface (T_s) was measured from the experimental condition of air and taken as 310 K. The ambient conditions were maintained in a closed room during experiments and ambient temperature of the surround–ding atmosphere (T_a) was measured as 294 K. By using the values T_a and Ts, the film temperature was calculated as:

$$T_f = \frac{T_s + T_a}{2} \tag{9}$$

From the above equation, T_f was calculated as 302 K. At 302 K, the value of volumetric thermal expansion (β) was noted as 3.31×10^3 K^{-1}. The fluid used for the experiments was natural air. However, the compu–ta–tional model was designed for methane (CH_4). Kine–matic viscosity of air (υ) was used as 17×10^{-6} m²/s, Prandtl number (Pr) = 0.7279, and thermal diffusivity (α) = 24×10^{-6} m²/s. These values were put in the FORTRAN program to perform the numerical simu–lations.

Results obtained for the vertical tube were validated by using the equation of the vertical plate. According to this equation, a vertically positioned cylinder can be preserved as a vertically positioned plate if it satisfies the criterion [18]:

$$\frac{d}{l} \geq \frac{34}{\sqrt[4]{Ra}} \tag{10}$$

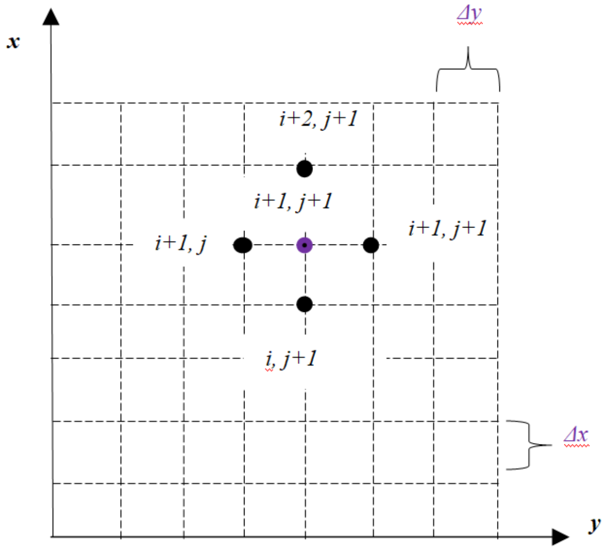

Figure 2. Grid of flow geometry

By following this equation, the following condition satisfies i.e. d/l = 0.0754 which was found lesser than 0.291. Eq. (10) does not satisfy the analytical model. So, it implicates that there are some obvious heat losses due to the effect of curvature and radiation.

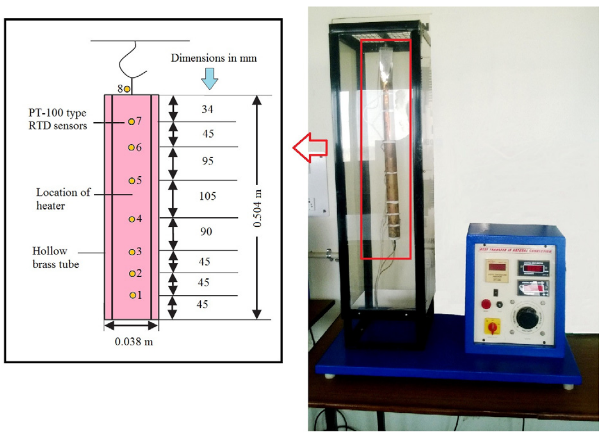

Figure 3. Natural convection equipment used for the experiments using air as a fluid

4. RESULTS AND DISCUSSION

In the previous section, the experimentation was done for the natural convection around the vertical tube using the air as a fluid. By using the experimentation data, further numerical simulations were done in order to obtain the numerical data. Numerical data was used to draw the results in the form of tables, charts, and graphs from the output of computer code. Numerical outputs were obtained in the form of velocity and temperature profiles which were used to obtain the hydrodynamic and thermal boundary layer thickness, respectively.

4.1 Velocity profiles

Velocity profiles and hydrodynamics boundary layer thickness of methane were studied for the different values of locations (x) on the vertical tube. Fig. 4 illustrates the velocity profiles for methane at different values of x. The boundary layer thickness is a function of kinematic viscosity and distance of a point from the leading edge. It is noticed that velocity (u) was observed minimum at $x = 0.1$ m however maximum at $x = 0.5$. As the vertical distance x (from bottom to top) increases, velocity (u) increases. Hence, the velocity curve at $x = 0.5$ m travels longer distance as compared to other profiles in the horizontal direction (y).

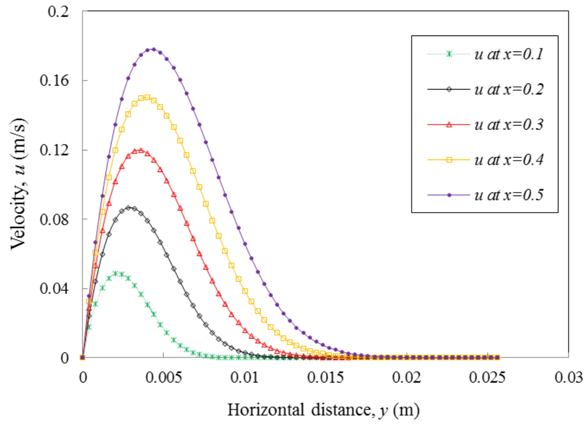

Figure 4. Velocity profiles for methane in vertical direction at various locations along heated vertical tube

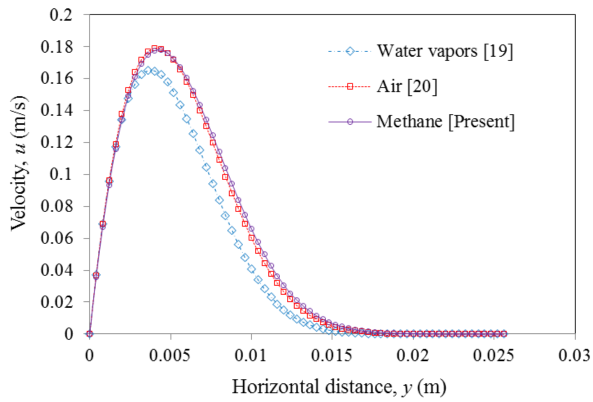

Figure 5. Comparison of velocity profiles of different fluids at location *x* = 0.5 m

Fig. 5 shows the velocity profiles for the methane, air [19], and water vapours [20] at $x = 0.5$ m. From these velocity profiles, the boundary layer thickness is calculated. From the difference between velocities profiles, it is observed that the velocity curve was approximately the same for air and methane because the kinematic viscosity of both fluids is the same but the curve peak and path in the case of water vapours is small. A similar trend was observed in the case of boundary layer thickness. The boundary layer thickness of water vapours was numerically observed as 0.0196 m, of air was 0.0208 m and of methane was 0.0216 m. Kinematic viscosity (υ) is physically equivalent to momentum diffusivity i.e. ability of particle to affect the momentum of adjacent particle. Therefore, a static particle nearby the static surface exerts a lesser obstruction effect as compared to that of a particle away from the static surface. However, the vapours of water feel a higher obstruction effect than air. Similarly, methane felt to a larger distance than air and water but the distance between methane and air is approximately the same because kinematic viscosity (υ) of both is approximately the same. Moreover, the velocity profiles demonstrate the effect of buoyancy. The $Pr < 1$ for methane indicates that the buoyant forces directly controlled the velocity profile. This effect was found to be lesser dominant in the case of air. However, the water vapours generated larger friction forces which tend to reduce the dominance of buoyant forces to some extent. Thus, the velocity profiles of air and water travel a smaller distance than methane. The characteristic of velocity profiles shows good agreement with the typical velocity characteristic curve for natural convection [21].

4.2 Hydrodynamics boundary layer thickness

The distance up to which the velocity gradient effects are significant is the Hydrodynamic boundary layer thickness (δ_H). As the velocity (u) approaches zero hydrodynamic boundary layer ends. Hydrodynamic boundary layer thickness (δ_H) directly depends upon velocity gradient.

The numerical data was generated from the output obtained from the computer code. Numerical data directly depends upon the initial parametric values of input and boundary-layer conditions. For the proof to be valid, the numerical results of the δ_H were compared with the analytical results calculated by using Von Karman's method of solving free convective heat transfer from a vertical cylinder to adjacent fluid [1]. According to this method, the boundary layer thickness can be calculated by [1]:

$$\frac{\delta_{anl(H)}}{x} = 3.93\frac{(\mathrm{Pr}+0.952)^{\frac{1}{4}}}{(\mathrm{Pr})^{\frac{1}{2}}\left(Gr_x\right)^{\frac{1}{4}}} \tag{11}$$

where the analytical hydrodynamic boundary layer thickness was denoted by $\delta_{anl(H)}$ (in m). Symbol Pr, Gr_x, and x are the Prandtl number, analytical Grashof num–ber, and vertical distance of the tube from the bottom to the top (x = 0.1, 0.2, 0.3, 0.4, and 0.5 m), respectively.

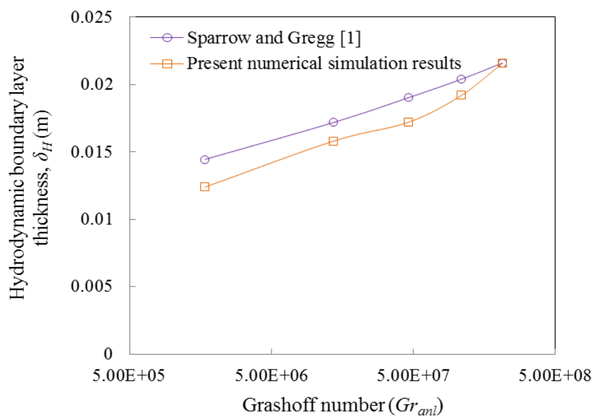

Figure 6. Numerical versus analytical δ_H with the variation in Grashof number for the fluid methane at various locations along with the heated vertical cylinder

From these velocity profiles, the hydrodynamic boundary layer thickness was calculated. Fig. 6 shows the boundary layer thickness for methane at different values of vertical distance (x). In Fig. 6, the numerical boundary layer thickness (δ_H) at x = 0.1 m was observed as 0.0124 m which was found minimum. At x = 0.2, 0.3, and 0.4 the value of δ_H was observed 0.0158, 0.0172, and 0.0192, respectively. At x = 0.5 m, numerical boundary layer thickness (δ_H) was observed 0.0216 m which was found maximum. Numerical boundary layer thickness at different points of x is given in Table 1. From Table 1, the general observation indicates that the value of δ_H increases with the value of the Grashof number (Gr). It was noticed that data between numerical hydrodynamic boundary layer thicknesses fall within the range of ±5% deviation with analytical boundary layer (±0.002 m).

Table 1. Summary of numerical and analytical δ_H

Parameter	x				
	0.1	0.2	0.3	0.4	0.5
Gr_x ($\times 10^6$)	1.7	13.6	45.9	108.8	212.2
$\delta_{H(anl)}$	0.0145	0.0172	0.0190	0.0204	0.0216
$\delta_{H(num)}$	0.0124	0.0158	0.0172	0.0192	0.0216

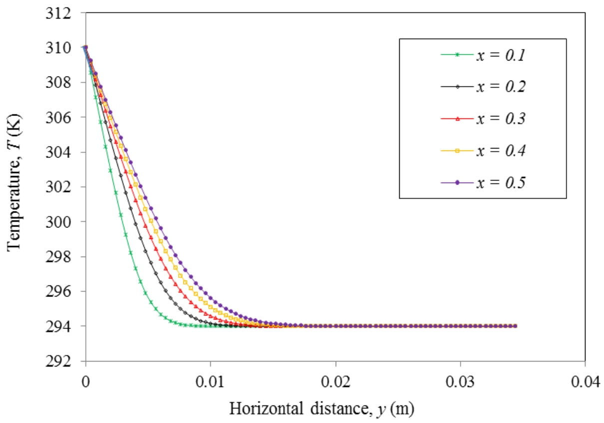

Figure 7. Temperature profiles for methane in the vertical direction at various locations along with the heated vertical cylinder

4.3 Temperature profiles

Fig. 7 illustrates the temperature profiles for methane at different values of x. Fig. 7 depicts that the temperature gradient drops with the value of x. From these profiles, thermal boundary layer thicknesses are calculated. Fig. 8 represents the temperature profiles of methane, air [19], and water vapours [20] at x = 0.5 m. From these temperature profiles, the thermal boundary layer thickness (δ_T) was calculated which is shown in Fig. 8. It was found that the temperature and velocity gradient travels longer distance in the y-axis as compared to the air and water vapours. At x=0.5 m, the value of δ_T was numerically observed as 0.0220 m for water vapours, 0.0260 m for air, and 0.0268 m for methane. The temperature profiles resemble the typical temperature characteristic curve for natural convection [21].

4.4 Thermal boundary layer thickness

The distance up to which the temperature gradient effects are significant is termed as thermal boundary layer thickness (δ_T). As the readings of temperature approach ambient temperature, the thermal boundary layer ends.

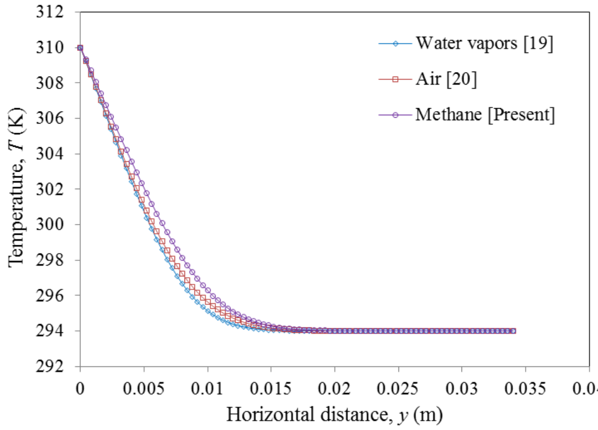

Figure 8. Comparison of temperature profiles of different fluids at location x = 0.5 m

Fig. 9 also shows the comparison between numerical and analytical boundary layer thickness. In Fig. 9, the numerical boundary layer thickness ($\delta_{T(num)}$) was found minimum at x = 0.1 and observed as 0.0142 m. At x = 0.2, 0.3, and 0.4 m, it was observed as 0.0176, 0.0208, and 0.0236 m respectively. At x = 0.5 m, numerical boundary layer thickness ($\delta_{T(num)}$) was observed maximum as 0.0260 m. For the proof of the results of thermal boundary layer thickness, we have an equation in which Prandtl number (Pr) is a connecting link between the velocity field and temperature, written as [17]:

$$\frac{\delta_T}{\delta_H} = \frac{1}{\sqrt{\mathrm{Pr}}} \tag{12}$$

Comparison between numerical and analytical vales of δ_T for methane at different points of x. is given in Table 2. Analytical δ_T observed at x = 0.1, 0.2, 0.3, 0.4, and 0.5 m was 0.0168, 0.0200, 0.0221, 0.0237, and 0.0251 m respectively. In Fig. 9, it is observed that data between numerical δ_T falls within in the range of ±5% deviation (±0.002 m) with analytical δ_T. Results of the numerical and experimental thermal and hydrodynamics boundary layers were found consistent and in good agreement.

Table 2. Comparisons between numerical and analytical thermal boundary layer thickness (δ_T)

Parameter	x				
	0.1	0.2	0.3	0.4	0.5
$\delta_{T(num)}$	0.0142	0.0176	0.0208	0.0236	0.0260
$\delta_{T(anl)}$	0.0168	0.0200	0.0221	0.0237	0.0251

It was also noticed that temperature falls early at x = 0.1 m. As the vertical distance (x) increases, a sudden decrease in the value of T drops. At point x = 0.5 m, the sudden fall of temperature was observed to be mini–mum. Hence, the temperature curve at x = 0.5 m travels more distance as compared to other profiles in the horizontal direction (y). Thermal boundary layer thickness directly depends upon temperature gradient.

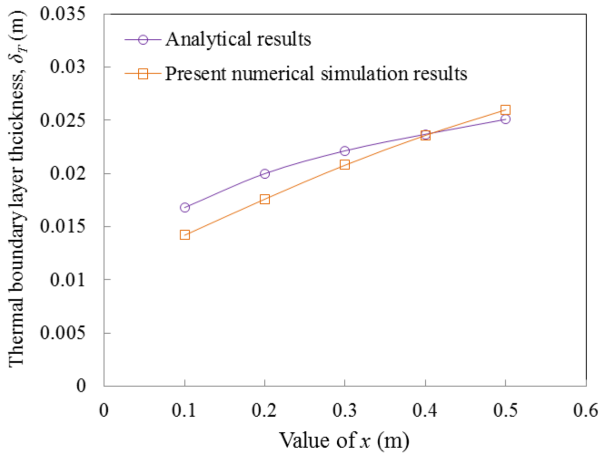

Figure 9. Comparison of numerical and analytical boundary layer thickness for methane

4.5 Nusselt number

From numerical data, various parameters related to fluid dynamics can be evaluated for instance Nusselt number, heat transfer coefficient (h), conduction heat (q), etc. By measuring the slope of temperature profiles for the various locations (x), the temperature gradient (dT/dy) was calculated. The temperature gradient dT/dy was calculated as 3353.50 2430.62, 2059.75, 1854.53, and 1681.81 K/m respectively at x = 0.1, 0.2, 0.3, 0.4, and 0.5 m. Convective heat transfer coefficient (h_x) can be used calculated by using the empirical relationship written as:

$$h_x = -k\frac{dT/dy}{T_s - T_a} \tag{13}$$

The value of h_x was calculated by using the k = 0.03228 W/mK i.e. the value of conductive heat transfer coefficient, surface temperature, and ambient temperature. The value of h_x can be utilized to evaluate the local Nusselt number (Nu_x). Nu_x was calculated by using the heat transfer coefficient (h_x), which is written as [22]:

$$Nu_x = \frac{h_x . x}{k} \tag{14}$$

In the above equation, the value of k was taken as 0.03228 W/mK. Churchill and Chu [23] also proposed a correlation for the calculation of Nu based on the Pr and Ra, written as:

$$Nu_x = 0.68 + \frac{0.67 Ra_x^{0.25}}{\left[1+\left(\frac{0.492}{\Pr}\right)^{\frac{9}{16}}\right]^{\frac{4}{9}}} \tag{15}$$

Present results of Ra and Pr satisfies the following condition: $0 < Ra_x < 10^9$ and $0 < Pr < \infty$ [24]. In the present study, the value of Ra lies in the range 1.24×10^6 to 1.54×10^8 which follows the condition of laminar flow i.e. $Ra \le 10^8$.

In the popular literature, another correlation is avai–lable which was proposed by McAdams [25], given as:

$$Nu_x = 0.59 \times Ra_x^{0.25} \tag{16}$$

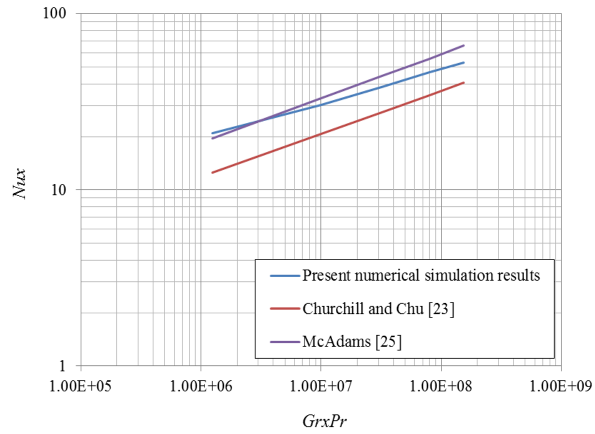

Figure 10. Analytical and numerical Nusselt number across the length of the vertical tube for the methane

The above equation is applicable to present results due to the agreement of condition: $10^4 < Ra_x < 10^9$. By using the Eq. (14–16), the present numerical results of Nu were compared with the analytical results. Fig. 10 shows the analytical and numerical values of local Nu across the length of the vertical tube for the methane. It was observed that the present results showed a good agreement with Churchill and Chu [23] and McAdams [25]. A new model (namely Jashanpreet and Chanpreet Model) has been proposed based on present results, given as:

$$Nu_x = 1.41 \times Ra_x^{0.19} \tag{17}$$

To test the above newly proposed model, the predicted data were plotted against the actual numerical results, and shows a good correlation coefficient (R^2) of 0.9989, as seen in Fig. 11.

4.6 Heat transfer coefficient

The value of convective h_x was evaluated as 6.76, 4.90, 4.15, 3.74, and 3.39 W/m^{2}K at x=0.1, 0.2, 0.3, 0.4, and 0.5 respectively. The direct average of h_x was evaluated as 4.59 W/m^{2}K. Fig. 12 indicates a variation in the values of numerically evaluated h_x with respect to constant values of analytical h_l. The average value of heat transfer coefficient along the overall length (h_l) was written as:

$$h_l = \frac{4}{3}\bar{h}_{x=l} \tag{18}$$

From the above equation, the h_l comes out as 6.12 W/m^{2}K (approximately) without consideration of any curvature effect.

According to Newton's law of cooling, the calcu–lation of analytical heat transfer coefficient can be done using the following equation [26]:

$$h_l = \frac{Q}{A(T_s - T_a)} \tag{19}$$

From the above equation, the value of Q was calculated from the experimental current and voltage values and calculated as 6.759 W. The analytical value of h_l was calculated as 6.76 W/m^{2}K (without any radiation loss). By comparison, the analytical and numerical values of h_l were found different. As men–tioned in Sec. 3, the value of the average heat transfer coefficient doesn't satisfy the equation of the plate, so there was a production of some radiation and curvature heat losses. To account for the effect of radiation loss, the following equation was used [27]:

$$q_{rad} = \sigma\varepsilon A\left(T_s^4 - T_a^4\right) \tag{20}$$

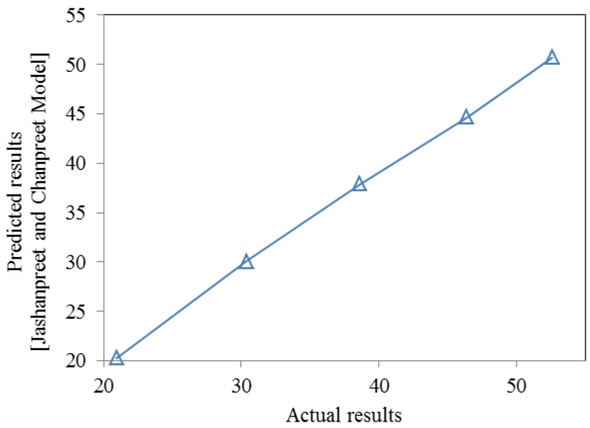

Figure 11. Actual versus predicted results of the newly proposed model of Nusselt number for numerical convection around vertical tube

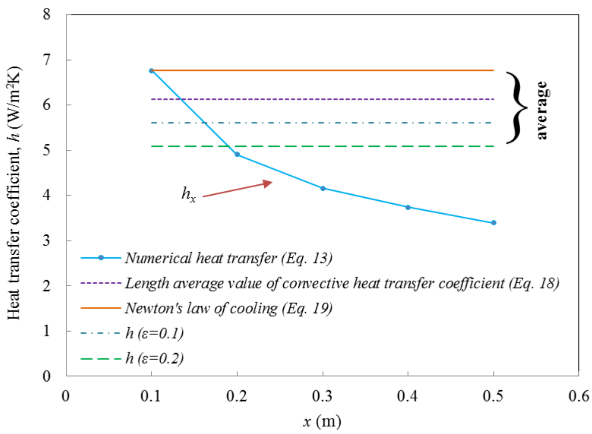

Figure 12. Variation of numerical heat transfer coefficient with respect to constant analytical heat transfer coefficient

In the above equation, the ε represents the emissivity of the brass tube that was taken as 0.1 and 0.2 for analysis purposes. To evaluate the effect of curvature loss, the curvature factor was calculated by using the following relationship [19]:

$$F = 1.3\left[\left(\frac{l}{d}\right)/Gr_{D=l}\right]^{0.25} + 1 \tag{21}$$

By using the above equation, the curvature factor (F) was calculated as 1.0265. Fig. 13 represents the heat transfer coefficient from the numerical and analytical results. Fig. 13 shows that by accounting for the curvature factor, the value of h_l changes to 5.09 W/m^{2}K which is lower than the actual average value of numerical h_l. However by taking the ε=0.1 and 0.2, the value of h_l changes to 5.67 and 5.09 W/m^{2}K, respect–tively. The value of h_l was found equal in the case of the effect of curvature and radiation loss (ε=0.2).

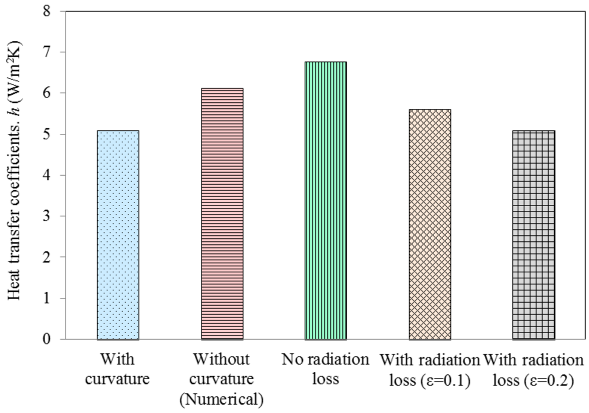

Figure 13. Heat transfer coefficient from the numerical and analytical results for methane

5. CONCLUSION

This study was carried out to numerically study the convective heat transfer across a vertical tube. Implicit scheme of finite difference method (FDM) was adopted numerically simulate the free convection phenomenon across vertical tube using LINUX based UBUNTU package. A FORTRAN code was run to successfully obtain the velocity profiles and temperature profiles. Numerical data were collected for the velocity, temperature profiles, boundary layer thickness (δ), Nusselt number (Nu), Rayleigh's number (Ra), and heat transfer coefficient (h). The following conclusions are drawn on the basis of numerical simulation results:

(i) By comparison of temperature profiles, it can be concluded that the temperature and velocity gradient travel longer distance in *the* direction perpendicular to the vertical tube as compared to the air and water vapours.

(ii) From the velocity profiles, the effect of buoyancy was demonstrated. The Pr < 1 for methane indicates that the buoyant forces directly controlled the velocity profile. This effect was found to be lesser dominant in the case of air. However, the water vapours generated larger friction forces which tend to reduce the dominance of buoyant forces to some extent. Thus, the velocity profiles of the air and water travel a smaller distance than methane.

(iii) Results of numerical and experimental thermal and hydrodynamics boundary layers were found to be consistent and in good agreement.

(iv) In the present study, the value of Ra lies in the range 1.24×10^6 to 1.54×10^8 which follows the condition of laminar flow i.e. $Ra \le 10^8$.

(v) The results of local Nusselt number (Nu) and boundary layer thickness showed a good agreement with the previous studies. The results of numerical

boundary layer thicknesses fall within the range of ±5% deviation with analytical boundary layer (±0.002 m).

(vi) Heat transfer coefficients found from the experimental and numerical study are also found to be in good agreement. Heat transfer coefficient (*h*) results indicate that there were some minor heat losses due to radiation of the brass tube and curvature of the tube.

ACKNOWLEDGMENT

The authors received no financial support for the research, authorship, and publication of this article.

REFERENCES

[1] E.M. Sparrow, J.L. Gregg, Laminar free convection heat transfer from the outer surface of a vertical circular cylinder, Transections ASME. 78 (1956) 1823–1829.

[2] J. Baliti, M. Hssikou, Y. Elguennouni, A. Moussaoui, M. Alaoui, Heat Transfer and Entropy Generation for Natural Convection by Adiabatic Obstacles Inside a Cavity Heated on the Left Side, FME Transtions Vol. 48, No 4, (2020) 825–832. doi:10.5937/fme2004825B.

[3] S. Acharya, S. Agrawal, S.K. Dash, Numerical Analysis of Natural Convection Heat Transfer from a Vertical Hollow Cylinder Suspended in Air, J. Heat Transfer. 140 (2018). https://doi.org/10.1115/1.4038478.

[4] D.M. Arshad, M. Inayat, I. Chughtai, Heat Transfer through Vertical Cylinder in Stationary Fluid, Nucl. 46 (2009) 177–188.

[5] T. Fujii, H. Uehara, Laminar natural convection heat transfer from the outer surface of a vertical cylinder, Int. J. Heat Mass Transf. 13 (1970) 607–615.

[6] K. Kitamura, A. Mitsuishi, T. Suzuki, F. Kimura, Fluid flow and heat transfer of natural convection induced around a vertical row of heated horizontal cylinders, Int. J. Heat Mass Transf. 92 (2016) 414–429. doi:10.1016/j.ijheatmasstransfer.2015.08.086.

[7] S.Ö. Atayilmaz, I. Teke, Experimental and numerical study of the natural convection from a heated horizontal cylinder, Int. Commun. Heat Mass Transf. 36 (2009) 731–738. doi: 10.1016/j.icheatmasstransfer.2009.03.017.

[8] S. Biswas, A.P. Kulkarni, S. Giddey, S. Bhattacharya, A Review on Synthesis of Methane as a Pathway for Renewable Energy Storage With a Focus on Solid Oxide Electrolytic Cell-Based Processes, Front. Energy Res. 8 (2020). https://doi.org/10.3389/fenrg.2020.570112.

[9] F.G. Blottner, Finite difference methods of solution of the boundary-layer equations, AIAA J. 8 (1970) 193–205. https://doi.org/10.2514/3.5642.

[10] S.C. Saha, M.A. Hossain, Natural Convection Flow with Combined Buoyancy Effects Due to Thermal and Mass Diffusion in a Thermally Stratified Media, Nonlinear Anal. Model. Control. 9 (2004) 89–102. doi:10.15388/na.2004.9.1.15173.

[11] M. Fahiminia, M.M. Naserian, H.R. Goshayeshi, D. Majidian, Investigation of Natural Convection Heat Transfer Coefficient on Extended Vertical Base Plates, Energy Power Eng. 03 (2011) 174–180. https://doi.org/10.4236/epe.2011.32022.

[12] S. Corasaniti, F. Gori, Natural convection around a vertical cylinder (thermal probe) immersed in a porous medium, Int. Commun. Heat Mass Transf. 81 (2017) 72–78. doi:10.1016/j.icheatmasstransfer.2016.12.006.

[13] L.J. Crane, Natural convection from a vertical cylinder at very small Prandtl numbers, Zeitschrift Für Angew. Math. Und Phys. ZAMP. 27 (1976) 61–70. https://doi.org/10.1007/BF01595242.

[14] M.K. Dash, S.K. Dash, Natural convection heat transfer and fluid flow around a thick hollow vertical cylinder suspended in air: A numerical approach, Int. J. Therm. Sci. 152 (2020) 106312. https://doi.org/10.1016/j.ijthermalsci.2020.106312.

[15] R.K. Deka, A. Paul, A. Chaliha, Transient free convection flow past vertical cylinder with constant heat flux and mass transfer, Ain Shams Eng. J. 8 (2017) 643–651. doi:10.1016/j.asej.2015.10.006.

[16] J.R. Senapati, S.K. Dash, S. Roy, Numerical investigation of natural convection heat transfer from vertical cylinder with annular fins, Int. J. Therm. Sci. 111 (2017) 146–159. doi:10.1016/j.ijthermalsci.2016.08.019.

[17] M. K, B. G., Advanced engineering fluid mechanics, Narosa Publishing House, New Delhi, 1996.

[18] J.C. Day, M.K. Zemler, M.J. Traum, S.K.S. Boetcher, Laminar natural convection from isothermal vertical cylinders: Revisting a classical subject, J. Heat Transfer. 135 (2013) 1–9. https://doi.org/10.1115/1.4007421.

[19] J. Singh, C. Singh, Numerical analysis of heat dissipation from a heated vertical cylinder by natural convection, Proc. Inst. Mech. Eng. Part E J. Process Mech. Eng. 231 (2017) 405–413. https://doi.org/10.1177/0954408915600109.

[20] J. Singh, C. Singh, S. Kumar, Implementation of Fuzzy Logic on FORTRAN coded free convection around vertical tube, Adv. Intell. Syst. Comput. 546 (2017) 331–341. https://doi.org/10.1007/978-981-10-3322-3_31.

[21] R.M. Darji, M.G. Timol, Similarity treatment for MHD free convective boundary layer flow of a class of Non-Newtonian fluids, FME Trans. 44 (2016) 197–203. doi: 10.5937/fmet1602197D.

[22] S.S. Goodrich, W.R. Marcum, Natural convection heat transfer and boundary layer transition for vertical heated cylinders, Exp. Therm. Fluid Sci. 105 (2019) 367–380. https://doi.org/10.1016/j.expthermflusci.2019.04.010.

[23] S.W. Churchill, H.H.S. Chu, Correlating equations for laminar and turbulent free convection from a vertical plate, Int. J. Heat Mass Transf. 18 (1975) 1323–1329. doi: 10.1016/0017-9310(75)90243-4.

[24] G. Habtay, J. Buzas, I. Farkas, Heat Transfer analysis in the chimney of the indirect solar dryer under natural convection mode, FME Trans. 48 (2020) 701–706. doi: 10.5937/fme2003701H.

[25] W.H. McAdams, Heat transmission, McGraw Hill, New York, 1954.
[26] J.G. Halpin, Newton’s law of cooling, Contemp. Phys. Play. 40 (1999) 205–212. doi:10.1080/001075199181549.
[27] E.E. Narimanov, I.I. Smolyaninov, Beyond Stefan-Boltzmann Law: Thermal, in: IEEE 2012 Conf. Lasers Electro-Optics, San Jose, CA, USA, 2012: pp. 2–3. https://doi.org/10.1364/qels.2012.qm2e.1.

NOMENCLATURE

d	Diameter of the tube [m]
g	Gravitational force [m^2/s]
Gr	Grashof number
h	Heat transfer coefficient [W/m^2.K]
i	Grid points in x direction
j	Grid points in y direction
k	Thermal conductivity [WK/m]
l	Length of the tube [m]
Nu	Nusselt number
Pr	Prendtl number
Ra	Rayleigh’s number
Q	Input heat [W]
T	Temperature [K]
u, v	Velocity components in Cartesian [m/s]
x	Locations on vertical tube [m]

Greek symbols)

δ	Boundary layer thickness [m]
v	Kinematic viscosity [m^2/s]
α	Thermal diffusivity [m^2/s]
β	Volumetric coefficient of thermal expansion [1/K]

Superscripts

a	Ambient
anl	Analytical
avg	Average
f	Film
l	Length
max	Maximum
num	Numerical
s	Surface
x	Location

РАЧУНСКА АНАЛИЗА КОНВЕКТИВНОГ ПРЕНОСА ТОПЛОТЕ ПРЕКО ВЕРТИКАЛНЕ ЦЕВИ

Ј. Синг, Ч. Синг

Рад приказује нумеричко истраживање конвективног преноса топлоте преко вертикалне цеви. За експеримент је коришћен ваздух као флуид у затвореном простору чиме је постигнут услов стационарног стања. Усвојена је имплицитна шема методе коначних резултата за нумеричку симулацију феномена слободне конвекције преко вертикалне цеви коришћењем Linuxa заснованог на Ubuntu. Нумерички подаци су се односили на брзину, температурне профиле, дебљину граничног слоја, Нуселтов број, Рајлијев број и коефицијент преноса топлоте. Резултати добијени за Нуселтов број су се слагали са резултатима објављеним у ранијим истраживањима. Коефицијент преноса топлоте показује незнатне губитке топлоте што је узроковала месингана цев и закривљеност цеви.